Superconductivity 18 (2026) 100257

Contents lists available at ScienceDirect

Superconductivity

journal homepage: www.sciencedirect.com/journal/superconductivity

Research Article

Method for three-dimensional I_c(θ,φ,B,T) anisotropy characterization of REBCO tapes using advanced torque magnetometry; experimental results at principal field anisotropies up to 45 T

R. Ries [a,*], J. Jaroszynski [b], D.C. Larbalestier [a,c]

[a] Applied Superconductivity Center, National High Magnetic Field Laboratory, Florida State University, Tallahassee, FL, 32310, USA
[b] Condensed Matter Science, National High Magnetic Field Laboratory, Florida State University, Tallahassee, FL, 32310, USA
[c] Department of Mechanical Engineering, FAMU-FSU College of Engineering, Tallahassee, FL, 32310, USA

A R T I C L E I N F O

Keywords:
Critical current evaluation
Three-dimensional field anisotropy
Torque magnetometry
REBCO CCs

A B S T R A C T

REBCO coated conductors (CCs) exhibit strong critical current anisotropy with respect to the magnetic field orientation relative to the tape plane, I_c(θ, φ), which is crucial for high-field applications such as fusion magnets operating in complex field geometries. Quantitative characterization of this anisotropy using transport measurements becomes increasingly challenging at low temperatures, high magnetic fields, and high critical currents. In this work, we introduce a torque-magnetometry-based method that extends the capability of the standard two-dimensional (2D) torque measurements I_c(θ) limited by fixed φ = 0° to full three-dimensional (3D) characterization I_c(θ, φ) with variable angle φ, as well as improves the accuracy of the evaluated critical currents. The study combines an analytical framework with redesigned torque probe components and is demonstrated experimentally up to 45 T. The effects of sample geometry, current redistribution, and intrinsic longitudinal–-transverse anisotropy are quantified and incorporated into the analysis. The experimental part focuses on principal field anisotropies, i.e. I_c(θ, 0°) and I_c(θ, 90°), corresponding to maximum (MLF) and variable Lorentz force (VLF) configurations, respectively. It was observed that their ratio follows higher-order angular dependence and increases with the applied magnetic field. The presented method enables rapid, non-destructive 3D anisotropy characterisation I_c(θ,φ,B,T) of the REBCO CCs in the temperature range 4.2 - 50 K and fields up to 45 T, extending anisotropy measurements into regimes difficult to access using conventional transport methods.

1. Introduction

REBCO ($REBa_2Cu_3O_{7-\delta}$) coated conductors (CCs) have become the most promising materials for next-generation superconducting technologies. Especially, REBCO CCs are leading candidates for high-field magnet technology in nuclear fusion reactors [1–6]. Despite major progress, REBCO CCs still present challenges. Their critical current (I_c) and related parameters remain difficult to determine accurately due to complex fabrication processes and variations between the samples. A major limitation is the lack of efficient, reliable characterization methods capable of mapping superconducting properties over a wide range of temperatures and all relevant field angles.

REBCO CCs also exhibit strong magnetic anisotropy – their I_c depends strongly on the magnetic field orientation relative to the tape plane [7–12]. This angular dependence is commonly expressed as I_c(θ, φ), where θ is the polar angle and φ is the azimuthal angle (Fig. 1a). The principal magnetic anisotropies in three-dimensional (3D) space are the maximum (MLF) and variable Lorentz force (VLF) configurations corresponding to φ = 0° and φ = 90°, respectively (Fig. 1b and c). The REBCO CCs anisotropy is particularly important in solenoidal and fusion-relevant magnet systems, such as tokamaks and stellarators [2,3,13,14], where the local magnetic field direction varies continuously along the conductor path. Accurate determination of I_c(θ, φ) at arbitrary field directions is therefore essential for conductor qualification, modelling, and optimized design for next-generation high-field magnet systems.

Until now, only a limited number of studies have reported measurements of angular magnetic field anisotropy in REBCO CCs [15–22]. Most existing techniques rely on transport measurements that require the injection of high currents into the REBCO tape at cryogenic

* Corresponding author.
E-mail address: rries@fsu.edu (R. Ries).

https://doi.org/10.1016/j.supcon.2026.100257
Received 16 January 2026; Received in revised form 6 April 2026; Accepted 19 April 2026
Available online 21 April 2026

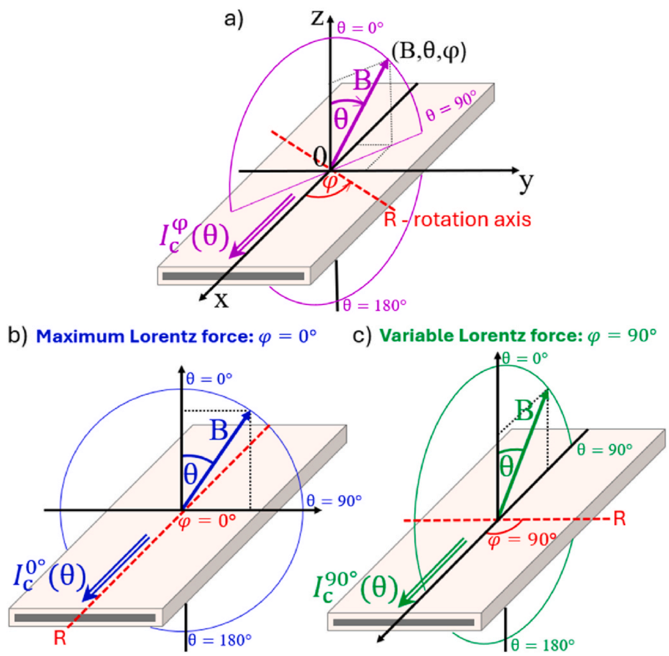

Fig. 1. *a) Definition of the polar angle θ and azimuthal angle φ used in torque magnetometry measurements. The polar angular dependence $I_c(\theta)$ is obtained by rotating the sample in the magnetic field while the azimuthal angle φ is variable but kept fixed during each measurement. The azimuthal angle φ is defined as the angle between the current direction and the rotation axis R. The detected current is always longitudinal with the sample length. Images b) and c) illustrate the principal field anisotropies corresponding to the maximum Lorentz force (φ=0°) and the variable Lorentz force (φ=90°), respectively.*

temperatures. Such measurements are technically demanding due to excessive Joule heating at current contacts, potential sample degradation, and difficulties in maintaining stable current flow in high-I_c conductors. In addition, these techniques often employ split-magnet systems, inherently limiting the achievable magnetic field strength to low or moderate levels.

In 2022, a patent entitled "*Magnetometer for Large Magnetic Moments with Strong Magnetic Anisotropy*" [23] introduced a torque magnetometry method for determining the angular critical current anisotropy of REBCO CCs under the MLF defined by I × B. Although this method successfully characterized the polar angular $I_c(\theta)$ dependence, its applicability was limited to a single azimuthal orientation $\varphi = 0°$. A subsequent study [24] reported good agreement with transport measurements, with deviations below 10% at magnetic fields up to 30 T, yet the comparison was performed on different samples cut from the same REBCO tape, which may exhibit longitudinal variability. More recent measurements show consistency between the two methods, with deviations below 5%.

The presented torque-magnetometry-based method introduces a principle and apparatus that extends the capability of standard 2D anisotropy scans $I_c(\theta)$ [24,25] to three-dimensional anisotropy characterization $I_c(\theta, \varphi)$ as well as improves the accuracy of the measured results. The method employs a modified torque magnetometer that allows rapid and non-destructive $I_c(\theta, \varphi)$ characterization across magnetic fields up to 45 T and temperature ranging from 4.2 K to 50 K providing a valuable tool for the next-generation high-field magnet systems.

2. Torque magnetometry

2.1. Advanced torque magnetometry probes

The principle of torque magnetometry setup has been described in detail previously [24,25]. For the present study, the sample platforms were redesigned to a square geometry and enlarged to their maximum feasible dimensions (Fig. 2). Two types of torque magnetometry probes are currently employed: a) a probe #1 designed for a 31 T resistive magnet equipped with a 20 × 20 mm^2 square platform, and b) a probe #2 developed for a hybrid magnet system at NHMFL operating at fields up to 45 T, equipped with a 12 × 12 mm^2 square platform. Thus, probe #1 can hold REBCO tapes up to 20 mm long, while probe #2 can hold tapes up to 12 mm long. The platforms of both probes are connected to enlarged precision pulleys compared to previous generation design [24,25], enabling highly accurate angular positioning. The square platform design, with screws at the corners, allows torque measurement on the sample positioned at any angle between the sample and the rotation axis, denoted φ (Fig. 3). This angle corresponds to the azimuthal angle between the field and the sample plane, as described in detail in the next chapter. During torque measurements, the sample is rotated recording polar angle dependence θ, while the azimuthal angle φ remains fixed for a given measurement. By repeating measurements at different azimuthal angles φ, access to the 3D characterization $I_c(\theta, \varphi)$ of the REBCO anisotropy is obtained. This study focuses on the principal field anisotropies corresponding to sample positioning at $\varphi = 0°$ and $\varphi = 90°$ (Fig. 3). In addition, each probe is equipped with small coils to accurately track the sample orientation with respect to the applied magnetic field, as well as integrated temperature sensors and heaters to perform measurements over a wide range of temperatures (4.2 K - 50 K).

2.2. Fundamentals of torque magnetometry

When a superconducting material is exposed to a magnetic field, shielding currents are induced in the loop to oppose the field penetration in accordance with Lenz's rule. In the case of a thin superconductor such as REBCO tape which is fully penetrated by a perpendicular oriented magnetic field [26], the induced loop current is distributed within the tape as illustrated in Fig. 4a. The loop current in the applied field produces a Lorentz force

$$\vec{F} = I\vec{L} \times \vec{B} \qquad \text{(eq. 1)}$$

where L represents the length of the current-carrying conductor exposed to the magnetic field.

When a rectangular REBCO tape rotates around its axis in the magnetic field B (Fig. 4), the part of the loop current I_{Loop} is parallel with the rotation axis $I_c^{\parallel R}$ and part is perpendicular to the rotation axis $I_c^{\perp R}$. Only the current component parallel to the rotation axis $I_c^{\parallel R}$ contributes to the torque. Torque can be then expressed:

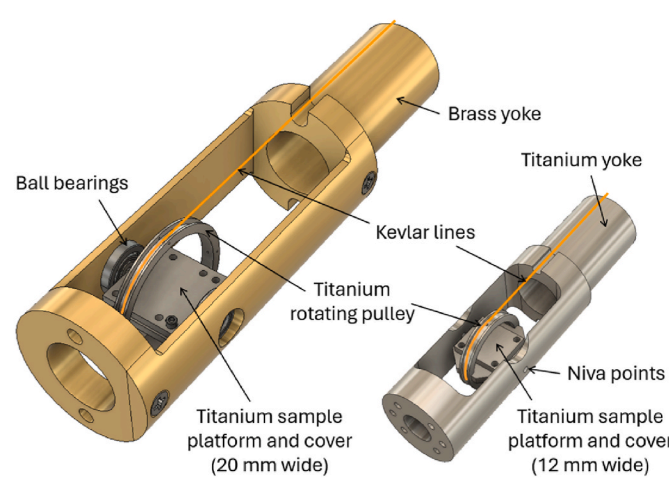

Fig. 2. *The illustration of the yokes of advanced torque magnetometry probes capable of 3D anisotropy characterization $I_c(\theta, \varphi)$ of the REBCO CCs. On the left is the yoke of probe #1, designed for operation in a 31 T resistive magnet, and on the right is the yoke of probe #2, designed for the 45 T hybrid magnet system at NHMFL.*

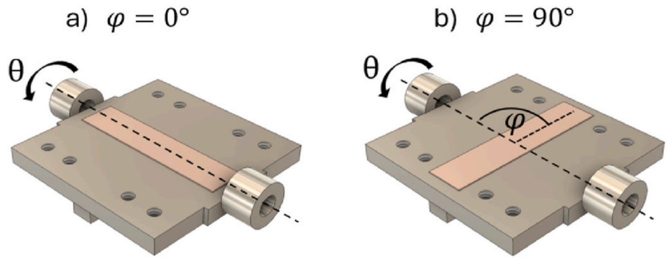

Fig. 3. *Illustration of the REBCO tape (18 × 4 mm²) mounted on the rotating platform of the torque magnetometer probe #1, showing the tape orientation a) parallel (φ = 0°) and b) perpendicular (φ = 90°) to the rotation axis. During torque measurements, the sample is pressed against the platform by a cover to ensure a fixed sample position.*

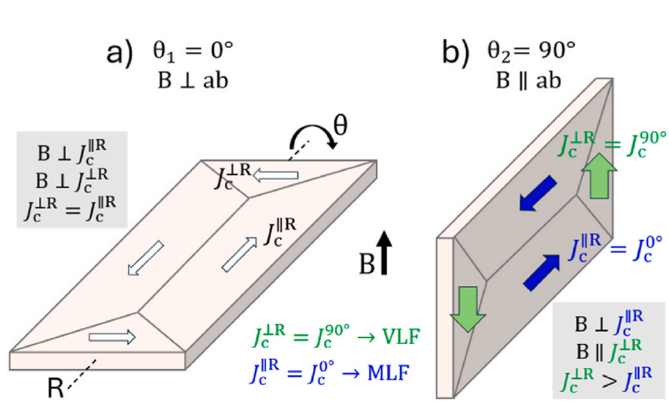

Fig. 4. *The illustration of the REBCO tape positioned at B⊥ab (a) and B ∥ab (b) showing change of current density components at two different sample orientations. The current density perpendicular to rotation axis varies according to variable Lorentz force $J_c^{\perp R} = J_c^{90^\circ}$, while current parallel to rotation axis according to maximum Lorentz force $J_c^{\parallel R} = J_c^{0^\circ}$.*

$$\vec{\tau} = \vec{r} \times \vec{F}$$

$$\tau = rF\sin(\theta) \qquad \text{(eq. 2)}$$

where r is the radius between the applied force (F) and the rotation axis, θ is the rotation (polar) angle between the force vector and the rotation axis.

While the currents parallel and perpendicular to rotation axis (R) are always the same $I_c^{\parallel R} = I_c^{\perp R}$, the current density components $J_c^{\parallel R}$ and $J_c^{\perp R}$ are changing differently, thus affecting the current distribution within the tape and the measured torque.

When the magnetic field B is perpendicular to the tape plane (Fig. 4a), both current density components, $J_c^{\parallel R}$ and $J_c^{\perp R}$ are perpendicular to the field: $B \perp J_c^{\parallel R}$, $B \perp J_c^{\perp R}$. For this particular case and assuming isotropic tape $J_c^{\parallel R} = J_c^{\perp R}$. As the tape rotates around its axis, parallel component $J_c^{\parallel R}$ varies according to the **maximum Lorentz force (MLF)** denoted $J_c^{0^\circ}$, thus $J_c^{\parallel R} = J_c^{0^\circ}$, while perpendicular component $J_c^{\perp R}$ follows the **variable Lorentz force (VLF)** denoted $J_c^{90^\circ}$, thus $J_c^{\perp R} = J_c^{90^\circ}$. At a field parallel to the tape plane (Fig. 4b), the current density component $J_c^{\parallel R}$ remains perpendicular to the field $B \perp J_c^{\parallel R}$ while $J_c^{\perp R}$ is now parallel to the field $B \parallel J_c^{\perp R}$ (Lorentz force free). In this particular case, the difference between the $J_c^{\perp R}$ and $J_c^{\parallel R}$ is the largest.

For the simplicity, **a principal anisotropy ratio** γ can be introduced as

$$\gamma(\theta) = \frac{J_c^{90^\circ}(\theta)}{J_c^{0^\circ}(\theta)} \qquad \text{(eq. 3)}$$

providing a quantitative measure of the tape's anisotropic behaviour at the principal field anisotropies. Both current densities, $J_c^{0^\circ}(\theta)$ and $J_c^{90^\circ}(\theta)$, increase as the tape rotates from angle $\theta_1 = 0^\circ$ to $\theta_2 = 90^\circ$ (Fig. 4) with $J_c^{90^\circ}(\theta)$ remaining dominant: $J_c^{90^\circ}(\theta) > J_c^{0^\circ}(\theta)$. As a consequence, the anisotropy ratio increases from $\gamma = 1$ at the angle θ_1 to its maximum $\gamma_{\max}$ at θ_2.

3. Torque at arbitrary field orientation

When measuring torque on rectangular superconducting sample oriented with its length parallel to the rotation axis $\boldsymbol{\tau^{0^\circ}}$ **(φ = 0°)** (Fig. 3a), the detected signal originates from the current component parallel to the rotation axis $I_c^{\parallel R}$ (yellow region in Fig. 5a). Since $J_c^{\parallel R} = J_c^{0^\circ}$ and cross-sectional area through which $I_c^{\parallel R}$ is flowing is in this configuration limited by tape width w, the $I_c^{\parallel R}$ is given by $J_c^{0^\circ}$:

$$I_c^{\parallel R} = J_c^{0^\circ} wt = I_c^{0^\circ} \qquad \text{(eq. 4)}$$

where t is the thickness of the REBCO layer. As the tape rotates from θ_1 to θ_2, the ratio $\gamma(\theta)$ increases changing current distribution within the tape by moving point A ($\gamma = 1$) to point B ($\gamma_{\max}$) as illustrated in Fig. 5a. The measured torque on rectangular superconducting sample at φ = 0° can be expressed using eqs. 1- 4, yielding:

$$\tau^{0^\circ} = 4BJ_c^{\parallel R} t\sin(\theta) \int_0^{\frac{w}{2}} y_{A\to B}(x)\cdot x\, dx$$

$$\tau^{0^\circ} = 4BJ_c^{\parallel R} t\sin(\theta) \int_0^{\frac{w}{2}} \left(\frac{x}{\gamma} + \frac{L}{2} - \frac{w}{2\gamma}\right) x\, dx$$

$$\tau^{0^\circ} = 4BJ_c^{\parallel R} t\sin(\theta) \left[\frac{2x^3}{3\gamma} + \frac{Lx^2}{4} - \frac{wx^2}{4\gamma}\right]_0^{\frac{w}{2}}$$

$$\tau^{0^\circ} = BJ_c^{0^\circ} t\sin(\theta)\frac{Lw^2}{4}\left(1 - \frac{w}{3L\gamma}\right) \qquad \text{(eq. 5)}$$

where $y_{A\to B}(x)$ is a linear function representing the change of current distribution within the tape expressing the shift of point A ($\gamma = 1$) to B ($\gamma_{\max}$) (Fig. 5a). The resulting solution for torque (eq. (5)) is equivalent to that expressed in Ref. [25]. From eq. (5), the parameter $J_c^{0^\circ}$ (and $I_c^{0^\circ}$) can simply be determined:

$$J_c^{0^\circ} = \frac{\tau^{0^\circ}}{Bt\sin(\theta)\frac{Lw^2}{4}\left(1 - \frac{w}{3L\gamma}\right)} \qquad \text{(eq. 6)}$$

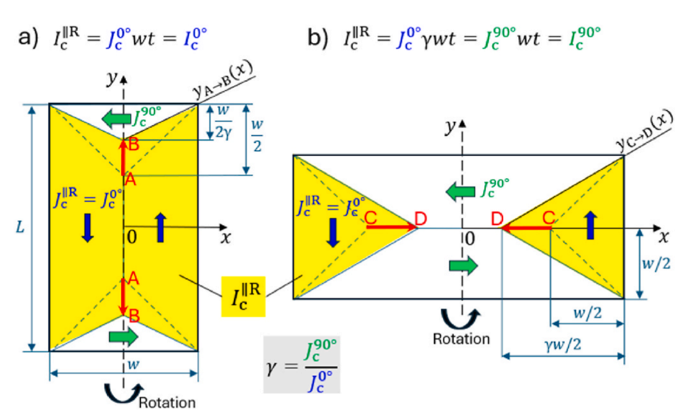

Fig. 5. *The illustration of the current distribution change in a rectangular REBCO tape during rotation from θ1 to θ2. Case a) tape positioned at φ = 0° and b) φ = 90°. The change of current distribution is indicated by moving points A→B and C→D, respectively. The measured torque originates from the current component parallel to the rotation axis (regions in yellow).*

When measuring torque on rectangular superconducting sample oriented with its length perpendicular to the rotation axis $\boldsymbol{\tau^{90^\circ}}$ **($\boldsymbol{\varphi = 90^\circ}$)** (Fig. 3b), the detected signal originates again from the current parallel to the rotation axis $I_c^{\|R}$ (yellow region in Fig. 5b). Yet $J_c^{\|R} = J_c^{0^\circ}$, the cross-sectional area through which $I_c^{\|R}$ is flowing is not in this configuration limited by tape width and $I_c^{\|R}$ **can increase** to equal bigger $J_c^{90^\circ} \cdot wt$ by a factor of anisotropy ratio γ. Thus, the $I_c^{\|R}$ is given by $J_c^{90^\circ}$:

$$I_c^{\|R} = J_c^{0^\circ} \gamma wt = J_c^{90^\circ} wt = I_c^{90^\circ} \quad \text{(eq. 7)}$$

As the tape rotates from θ_1 to θ_2, the ratio γ increases changing current distribution within the tape by moving point C ($\gamma = 1$) to point D ($\gamma_{\max}$) as illustrated in Fig. 5b. The measured torque on rectangular superconducting sample at $\varphi = 90^\circ$ can be determined by following integral and solution:

$$\tau^{90^\circ} = 4BJ_c^{\|R} t \sin(\theta) \int_{\frac{1}{2}(L - w\gamma)}^{\frac{L}{2}} y_{C\rightarrow D}(x) \cdot x \, dx$$

$$\tau^{90^\circ} = 4BJ_c^{\|R} t \sin(\theta) \int_{\frac{1}{2}(L - w\gamma)}^{\frac{L}{2}} \left(\frac{x}{\gamma} + \frac{w}{2} - \frac{L}{2\gamma} \right) x \, dx$$

$$\tau^{90^\circ} = 4BJ_c^{\|R} t \sin(\theta) \frac{1}{2\gamma} \left[\frac{2x^3}{3} + \frac{x^2(w\gamma - L)}{2} \right]_{\frac{1}{2}(L - w\gamma)}^{\frac{L}{2}}$$

$$\tau^{90^\circ} = BJ_c^{0^\circ} t \sin(\theta) \frac{\gamma L w^2}{4} \left(1 - \frac{\gamma w}{3L} \right)$$

$$\tau^{90^\circ} = BJ_c^{90^\circ} t \sin(\theta) \frac{L w^2}{4} \left(1 - \frac{\gamma w}{3L} \right) \quad \text{(eq. 8)}$$

where $y_{C\rightarrow D}(x)$ is a linear function representing the change of current distribution within the tape expressing the shift of point C ($\gamma = 1$) to D ($\gamma_{\max}$) (Fig. 5b). From eq. (8), $J_c^{90^\circ}$ (and $I_c^{90^\circ}$) can be determined:

$$J_c^{90^\circ} = \frac{\tau^{90^\circ}}{Bt \sin(\theta) \frac{Lw^2}{4} \left(1 - \frac{w\gamma}{3L} \right)} \quad \text{(eq. 9)}$$

The **terms in brackets** in eqs. (6) and (9) represent a **geometrical factor** reflecting **current distribution** within the tape ends and **ratio $\boldsymbol{\gamma}$** in these terms reflect **change of current distribution** during tape rotation. As can be seen, the ratio γ has only a minor effect on measured torque τ (and thus on the evaluated $J_c^{0^\circ}$ and $J_c^{90^\circ}$) and its influence decreases with sample aspect ratio L/w.

When measuring torque on rectangular sample at $\varphi = 90^\circ$ (τ^{90°), certain conditions may cause the detected torque signal may not originate directly from $J_c^{90^\circ}$. This may occur when the sample's aspect ratio L/w is lower than anisotropy ratio $\gamma_{\max}$, $L/w < \gamma_{\max}$ (Fig. 6). During the sample rotation, ratio γ increases, moving point C to the new position D consistent with eq. (8) until point D reaches the center of the sample. Beyond this angle, point D can no longer shift laterally and instead moves vertically to a new position E when the measured signal begins to behave analogously to eq. (5). In this scenario, the measured torque (τ^{90°) doesn't fully originate from $J_c^{90^\circ}$ during the entire rotation from θ_1 to θ_2. Considering the typical properties of REBCO tapes ($\gamma \approx$ 1-1.5) and the standard sample dimensions used in our torque magnetometers ($L/w \approx$ 2-5), this situation cannot be reached.

In summary, the critical current $I_c(\theta, \varphi)$ evaluated from the torque measurements always correspond to the current flowing along the longer dimension (L) of the rectangular sample. The azimuthal angle φ corresponds to the sample position on the platform of the torque magnetometer which is the angle between the sample length and the

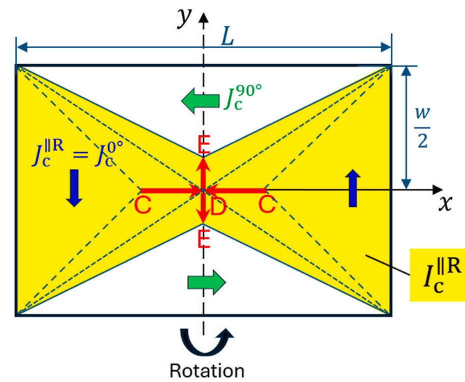

Fig. 6. *The illustration of the current distribution change in a rectangular REBCO tape with $L/w < \gamma_{max}$ at $\varphi = 90^\circ$ during rotation from θ_1 to θ_2. The change of current paths is indicated by moving points C→D→E.*

rotation axis. The sample position at $\varphi = 0^\circ$, corresponds to the magnetic anisotropy at MLF, while $\varphi = 90^\circ$ corresponds to magnetic anisotropy at VLF. Considering this, the $I_c(\theta, \varphi)$ anisotropy of any superconducting material can be characterized at any field orientation relative to the sample plane, provided that an appropriate sample geometry is used and the sample is suitably mounted on the rotating platform of the torque magnetometer.

4. Influence of change of current distribution on torque τ

As shown, the sample rotation causes a change in the current density components leading to a redistribution of current within the tape, i.e. moving points A→B and C→D in Fig. 5. This redistribution directly influences the measured torques (τ^{0° and τ^{90°) and thus evaluated $J_c^{0^\circ}$ and $J_c^{90^\circ}$. To quantify this effect, only the bracketed terms in eqs. (6) and (9) can be compared with anisotropy ratio ($\gamma > 1$) and neglecting it ($\gamma = 1$), thus

$$J_c^{0^\circ} \sim \frac{1}{\left(1 - \frac{w}{3L\gamma} \right)} \quad \text{(eq.10)}$$

$$J_c^{90^\circ} \sim \frac{1}{\left(1 - \frac{w\gamma}{3L} \right)} \quad \text{(eq.11)}$$

Fig. 7a shows calculated normalised $J_c^{0^\circ}$ (eq. (10)) and $J_c^{90^\circ}$ (eq. (11)) as a function of the sample aspect ratio L/w for several γ values relevant for REBCO tapes. Fig. 7b shows the ratio between J_c components with ($\gamma > 1$) and without ($\gamma = 1$) the inclusion of the ratio γ. As shown in the plot, increasing the L/w ratio reduces the influence of the ratio γ on both $J_c^{0^\circ}$ and $J_c^{90^\circ}$. Conversely, the higher the ratio γ, the stronger its influence becomes. Neglecting the ratio γ leads to an overestimation of $J_c^{0^\circ}$ and an underestimation of $J_c^{90^\circ}$. As can be seen, the ratio γ influences $J_c^{90^\circ}$ more strongly than $J_c^{0^\circ}$.

For the standard sample aspect ratios used in presented torque magnetometers ($L/w \approx$ 3-5, probe #1) and typical REBCO properties ($\gamma \approx$ 1-1.5), neglecting the ratio γ can cause an overestimation of $J_c^{0^\circ}$ by up to 4% and underestimation of $J_c^{90^\circ}$ by up to 7% at their peak positions. In contrast, for anisotropic REBCO tapes, particularly those exhibiting peak shifts (such as THEVA tape [8,27]), the ratio γ may locally exhibit values by up to $\gamma \approx 1.8$ and particularly when measuring with the probe designed for 45 T hybrid magnet system where the maximum useable sample length is limited to 12 mm ($L/w \leq 3$), the $J_c^{0^\circ}$ and $J_c^{90^\circ}$ deviations caused by neglecting the ratio γ may overcome 6% and 11%, respectively. Therefore, for low aspect ratio samples or strongly anisotropic conductors, it is essential to determine the ratio $\gamma(\theta)$ from torque data and incorporate it into the evaluation of $J_c^{0^\circ}(\theta)$ and $J_c^{90^\circ}(\theta)$ leading to

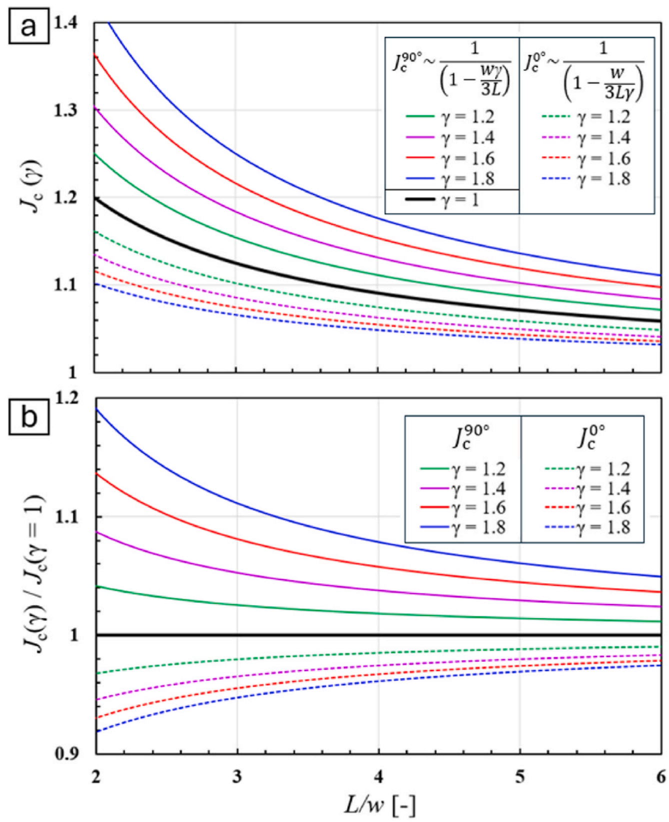

Fig. 7. *a) Normalised $J_c^{0°}$ and $J_c^{90°}$ values as a function of the sample aspect ratio L/w relevant for torque magnetometry measurements, b) the ratio between J_c components with ($\gamma > 1$) and without ($\gamma = 1$) the inclusion of the ratio γ. In the plots, several γ values relevant for typical REBCO tapes were used. The data calculated from eqs.* (10) and (11).

more accurate results.

5. Evaluation of anisotropy ratio γ from torque data

The anisotropy ratio γ can be determined from torque data comparing $\tau^{90°}$ (eq. (8)) and $\tau^{0°}$ (eq. (5)) yielding to cubic function:

$$\frac{\tau^{90°}}{\tau^{0°}} = \frac{\gamma\left(1-\frac{\gamma w}{3L}\right)}{\left(1-\frac{w}{3L\gamma}\right)} \quad \text{(eq.12)}$$

Applying the substitution $\frac{w}{3L} = j$, the function yields:

$$\frac{\tau^{90°}}{\tau^{0°}} = \frac{\gamma(1-\gamma j)}{\left(1-\frac{j}{\gamma}\right)} \quad \text{(eq. 13)}$$

$$\gamma^3 j - \gamma^2 + \frac{\tau^{90°}}{\tau^{0°}}(\gamma - j) = 0$$

The solution for this function can be found analytically using the Cardano transformation with discriminant

$$\Delta = \left(\frac{q}{2}\right)^2 + \left(\frac{p}{3}\right)^3$$

and radicals

$$A = \sqrt[3]{-\frac{q}{2} + \sqrt{\Delta}}, B = \sqrt[3]{-\frac{q}{2} - \sqrt{\Delta}}$$

with

$$q = -\frac{2}{27j^3} + \frac{\tau^{90°}}{\tau^{0°}}\left(\frac{1}{3j^2} - 1\right), p = \frac{1}{j}\left(\frac{\tau^{90°}}{\tau^{0°}} - \frac{1}{3j}\right)$$

The three solutions are then

$$\gamma_n = \omega^n A + \omega^{2n} B + \frac{1}{3j}, n = 0, 1, 2 \quad \text{(eq. 14)}$$

with $\omega = e^{-2\pi i/3}$.

Although the cubic equation offers an exact analytical solution, its explicit form contains nested radicals, cube roots and imaginary components, making parameter extraction highly sensitive to numerical instability in practical data evaluation. Considering this, substituting γ in denominator in eq. (12) by $\gamma \approx \frac{\tau^{90°}}{\tau^{0°}}$, where its effect is minimal, the cubic function yields the simplified quadratic form, whose accuracy improves with increasing L/w ratio. The resulting function and corresponding solutions are as follows:

$$\frac{\tau^{90°}}{\tau^{0°}} = -\gamma^2 j + \gamma + j \quad \text{(eq. 15)}$$

$$\gamma_{1,2} = \frac{1 \pm \sqrt{1 + 4j\left(j - \frac{\tau^{90°}}{\tau^{0°}}\right)}}{2j} \quad \text{(eq. 16)}$$

For samples with very large aspect ratio, i.e. $L \gg w$, the influence of the ratio γ in both bracketed terms in eq. (12) becomes negligible, allowing its determination directly from torque data yielding to simple linear form:

$$\frac{\tau^{90°}}{\tau^{0°}} = \gamma \quad \text{(eq. 17)}$$

Fig. 8a shows the comparison between cubic, quadratic and linear functions, i.e. eqs. (13), (15) and (17). Fig. 8b shows relative comparison between the cubic and quadratic forms as a function of ratio γ for several relevant sample aspect ratios L/w.

As can be seen, the linear function provides only a very rough approximation of ratio γ and can bring deviation by up to $\gamma = n \pm 20\%$ for even the maximum sample dimensions useable for presented torque magnetometers. In contrast, the quadratic approximation shows strong consistency with the cubic function. For even using a relatively short sample limited by space of probe #2 ($L/w \approx$ 2-3) and assuming an extremely high anisotropy ratio $\gamma = 2$, the quadratic approximation shows an accuracy above 97%. For standard samples with $L/w \approx$ 3-5, which can be mounted on probe #1, the accuracy further improves to above 99%. Since the cubic term introduces only a minor correction, the quadratic model captures the dominant physical behaviour without introducing noticeable errors. Therefore, for practical data evaluation, the quadratic approximation is sufficient and preferable.

Fig. 8a also shows that for a given REBCO tape with a certain ratio γ, the difference between the measured torques $\tau^{90°}$ and $\tau^{0°}$ increases with increasing sample aspect ratio L/w. Similarly, for samples with identical aspect ratio L/w, the difference between $\tau^{90°}$ and $\tau^{0°}$ becomes larger as the ratio γ is bigger.

6. Influence of longitudinal and transverse J_c anisotropy

Let's consider REBCO tape with natural longitudinal (along the length) and transverse (across the width) current anisotropy ($J_c^L \neq J_c^T$). The degree of longitudinal and transverse anisotropy can, for simplicity, be characterized by a ratio η:

$$\eta = \frac{J_c^L}{J_c^T} \quad \text{(eq. 18)}$$

When the sample is mounted on a platform at φ = 0° (Fig. 3a), the

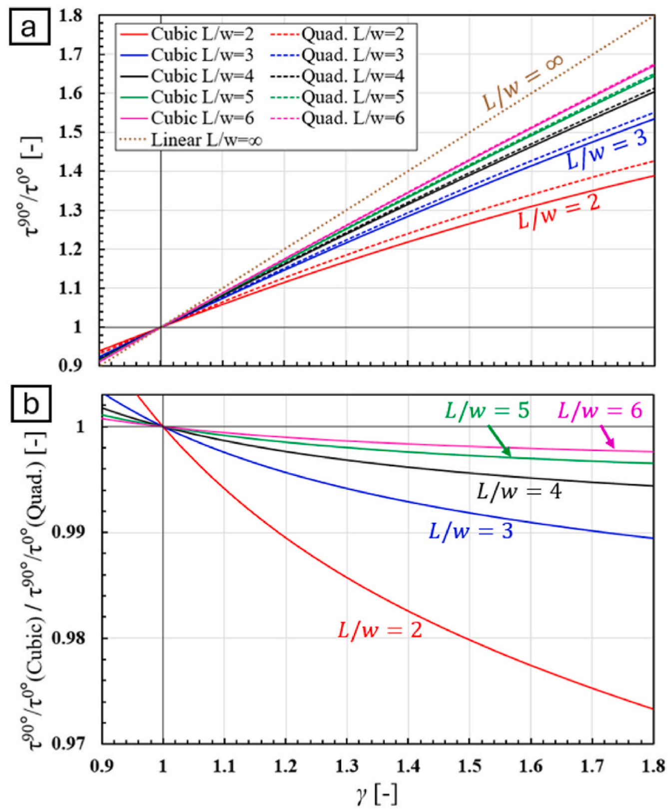

Fig. 8. *a) Comparison of cubic, quadratic and linear functions of ratio γ, and b) relative comparison between cubic form and quadratic approximation as a function of ratio γ for different sample aspect ratios L/w. The data calculated from eqs. (12)–(17).*

measured torque signal (τ^{0°) originates from the longitudinal current which is subject to the MLF: $J_c^{L0^\circ}$, regardless of ratio η. Similarly, at $\varphi = 90^\circ$ (Fig. 3b), the torque signal (τ^{90°) originates from the longitudinal current which is subject to the VLF: $J_c^{L90^\circ}$, regardless of ratio η. The transverse component J_c^{T} and thus ratio η can also be determined using torque magnetometry by preparing a sample where the width of the tape is the sample's longest dimension allowing measurement of $J_c^{T0^\circ}$ and $J_c^{T90^\circ}$ which will be part of the investigation in our further study.

However, during the torque measurements, the ratio η affects the current distribution within the tape in both configurations. The effect of ratio η can be incorporated into eqs. (6) and (9) resulting in their modified forms:

$$J_c^{0^\circ} = \frac{\tau^{0^\circ}}{Bt\,\sin(\theta)\,\frac{Lw^2}{4}\left(1 - \frac{w\eta}{3L\gamma}\right)} \qquad \text{(eq. 19)}$$

$$J_c^{90^\circ} = \frac{\tau^{90^\circ}}{Bt\,\sin(\theta)\,\frac{Lw^2}{4}\left(1 - \frac{w\eta\gamma}{3L}\right)} \qquad \text{(eq. 20)}$$

Thus, the ratio η enhances the contribution of the bracketed terms, but its effect decreases with increasing sample aspect ratio L/w. For most of the REBCO tapes $\eta \approx 1$ having negligible effect on evaluated $J_c^{0^\circ}$ and $J_c^{90^\circ}$ results. In contrast, for samples deposited by inclined substrate deposition (ISD) techniques like THEVA, the ratio $\eta > 1.3$ [27] and should be incorporated into the evaluation of $J_c^{0^\circ}$ and $J_c^{90^\circ}$ to improve the accuracy of the measured results.

7. Experimental results

In the experimental part, two different commercial REBCO tapes, denoted S1 manufactured by SuperMag Technology (Shanghai) Co., Ltd. and S2 manufactured by Faraday Factory Japan LLC, were investigated using torque magnetometry probes #1 and #2, respectively. All measurements were performed at the temperature of 4.2 K. Magnetic fields up to 30 T were applied using probe #1, while probe #2 enabled measurements at 45 T. The samples had rectangular geometries with dimensions of S1: 15.2 × 4 mm^2 and S2: 10.6 × 4 mm^2, corresponding to aspect ratios $L/w = 3.8$ and 2.65, respectively.

Fig. 9 shows the principal critical currents, $I_c^{0^\circ}(\theta)$ and $I_c^{90^\circ}(\theta)$ (primary axis), for sample S1, evaluated from torque measurement τ^{0° and τ^{90° (secondary axis) at 4.2 K and a magnetic field of 10 T. The lower part of the image shows the evaluated ratio γ(θ), determined both directly from the torque data using the quadratic function (eq. (15)) and from the evaluated critical currents (eq. (3)) showing nearly identical angular dependences, demonstrating the consistency of the evaluation methods. The solid line corresponds to fit of the evaluated data points.

As expected, $I_c^{90^\circ}(\theta)$ exceeds $I_c^{0^\circ}(\theta)$ over the entire angular range. Both critical currents exhibit the same value only at the polar angle $\theta = 0^\circ$, when the magnetic field is perpendicular to the tape plane for any azimuthal angle φ. The biggest difference between the $I_c^{90^\circ}(\theta)$ and $I_c^{0^\circ}(\theta)$ occurs at $\theta = 90^\circ$. At this orientation, the sample in VLF configuration approaches the Lorentz force free condition, whereas in the MLF configuration the Lorentz force remains maximal. Consequently, the anisotropy ratio reaches its maximum value $\gamma_{max} = 1.13$.

In both configurations, the angular dependence of the critical current is primarily governed by the intrinsic anisotropy of the REBCO, including its layered crystal structure, grain misalignment, and pinning landscape [28–30]. These properties affect the REBCO critical current in both configurations in a similar way and can be represented by a common angular factor $I_{c0}(\theta)$. The $I_c^{0^\circ}(\theta)$ and $I_c^{90^\circ}(\theta)$ can therefore be expressed as

$$I_c^{0^\circ}(\theta) = I_{c0}(\theta) \qquad \text{(eq. 21)}$$

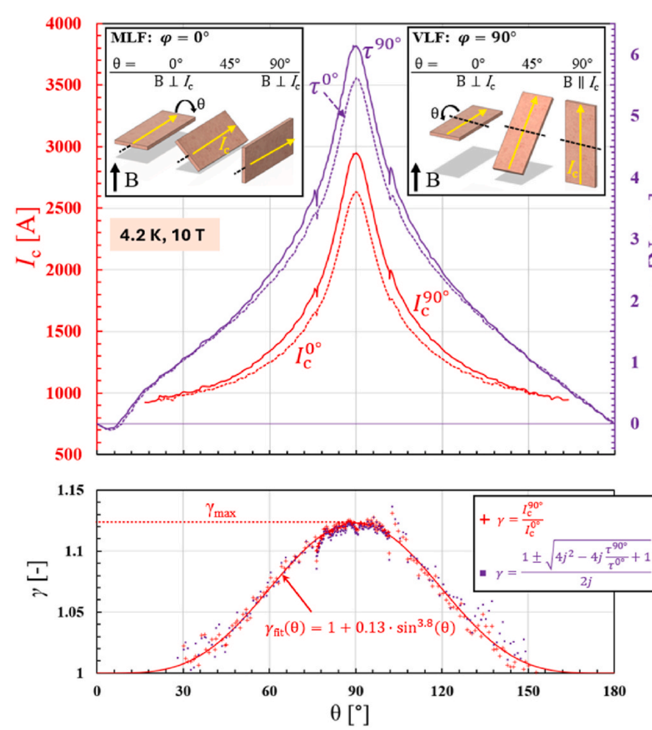

Fig. 9. *The principal critical currents, $I_c^{0^\circ}(\theta)$ and $I_c^{90^\circ}(\theta)$, of the sample S1 evaluated from the torque signals τ^{0° and τ^{90°, measured at 4.2 K and 10 T. The lower part shows the anisotropy ratio $\gamma(\theta)$ determined from the torque signals using a quadratic approximation (purple points) and from the evaluated critical currents (red points). The solid line corresponds to fit of the experimental data.*

$$I_c^{90^\circ}(\theta) = I_{c0}(\theta) + \Delta I_c(\theta) \quad \text{(eq. 22)}$$

The additional term $\Delta I_c(\theta)$ at VLF configuration reflects the extra critical current given by reduced Lorentz force. Thus

$$\gamma(\theta) = \frac{I_{c0}(\theta) + \Delta I_c(\theta)}{I_{c0}(\theta)} = 1 + \frac{\Delta I_c(\theta)}{I_{c0}(\theta)} \quad \text{(eq. 23)}$$

demonstrating that the anisotropy ratio $\gamma(\theta)$ effectively removes the dominant intrinsic angular anisotropy and isolates the additional term for critical current enhancement $\Delta I_c(\theta)/I_{c0}(\theta)$. As the Lorentz force reduction scales as $F \propto JB\sin(\theta)$, it introduces an angular dependence on $\sin(\theta)$ leading to general expression

$$\frac{\Delta I_c(\theta)}{I_{c0}(\theta)} = C(B)\sin^n(\theta) \quad \text{(eq. 24)}$$

and thus

$$\gamma(\theta) = 1 + C(B)\sin^n(\theta) \quad \text{(eq. 25)}$$

with

$$C(B) = \gamma_{max}(B) - 1 \quad \text{(eq. 26)}$$

where, C(B) represents the strength of vortex motion suppression, and the exponent n represents an effective order of Lorentz force suppression.

As observed from Fig. 9, $\gamma_{max} = 1.13$ corresponding to C(10 T) = 0.13. This leads to a critical current enhancement $\Delta I_c(\theta)/I_{c0}(\theta) = 13\%$ and an extra critical current $\Delta I_c \approx 330$ A at VLF configuration and Lorentz force free orientation ($\theta = 90^\circ$).

The measurements performed at higher magnetic fields (Fig. 10), including sample S1 measured at 5, 10, 20, and 30 T and sample S2 measured at 45 T, demonstrate that the maximum anisotropy ratio γ_{max}, and consequently coefficient C, increase with the field, as expected. The n-exponent was determined from power function fits in log–log plots of $\gamma(\theta)-1$ versus $\sin(\theta)$ shown in Fig. 11a. Fig. 11b shows field dependence of γ_{max} (primary axis) and the n-exponent (secondary axis) for samples S1 and S2. For sample S1, γ_{max} increases with the magnetic field and tends to saturate at higher fields. The n-exponent decreases from n(5 T) ≈ 4.2 to n(30 T) ≈ 3.2. The observed higher-order angular dependence indicates the presence of multiple angular contributions to $\Delta I_c(\theta)$ as the Lorentz force is reduced. The resulting extra critical current $\Delta I_c(\theta)$ is increasing with the magnetic field and tends to saturate as expected.

Sample S2, measured at 45 T, exhibits an even larger value of γ_{max}, and thus coefficient C with smaller n-exponent, consistent with the trends observed for sample S1, however, as this tape originates from a different manufacturer a direct quantitative comparison is not appropriate. While the presented γ_{max}(B), thus C(B) and n(B) data capture the basic trends, additional measurements would be required to establish the full functional dependence of all parameters.

The symmetric peak positions of both $I_c^{0^\circ}$ and $I_c^{90^\circ}$ at $\theta = 90^\circ$ demonstrate a highly oriented REBCO crystalline structure in both samples S1 and S2, with minimal crystallographic misalignment relative to the substrate plane.

Applying the anisotropy ratio $\gamma(\theta)$ into the evaluation of $I_c^{0^\circ}(\theta)$ and $I_c^{90^\circ}(\theta)$ has the largest effect when the ratio $\gamma(\theta)$ is maximal. For sample S1 ($L/w = 3.8$) with $\gamma_{max} \approx 1.2$ at 30 T, this resulted in a decrease of $I_c^{0^\circ}(90^\circ)$ by approximately 1.5% and increase of $I_c^{90^\circ}(90^\circ)$ by about 2% corresponding to negligible corrections. In contrast, for sample S2 with lower aspect ratio $L/w = 2.65$ and higher ratio $\gamma_{max} \approx 1.3$, the corrections are more pronounced, leading to a decrease of $I_c^{0^\circ}(90^\circ)$ by about 4% and an increase of $I_c^{90^\circ}(90^\circ)$ by 6%.

Based on the analytical framework and the representative experimental results at principal field anisotropies, we demonstrated the validity and effectiveness of the torque-magnetometry-based method for 3D anisotropy characterisation $I_c(\theta, \varphi, B, T)$ with fixed in-plane current direction. In future work, this approach will be extended to full 3D mapping of the critical current anisotropy over multiple azimuthal angles φ, enabling a comprehensive characterization of REBCO tapes under arbitrary field orientations.

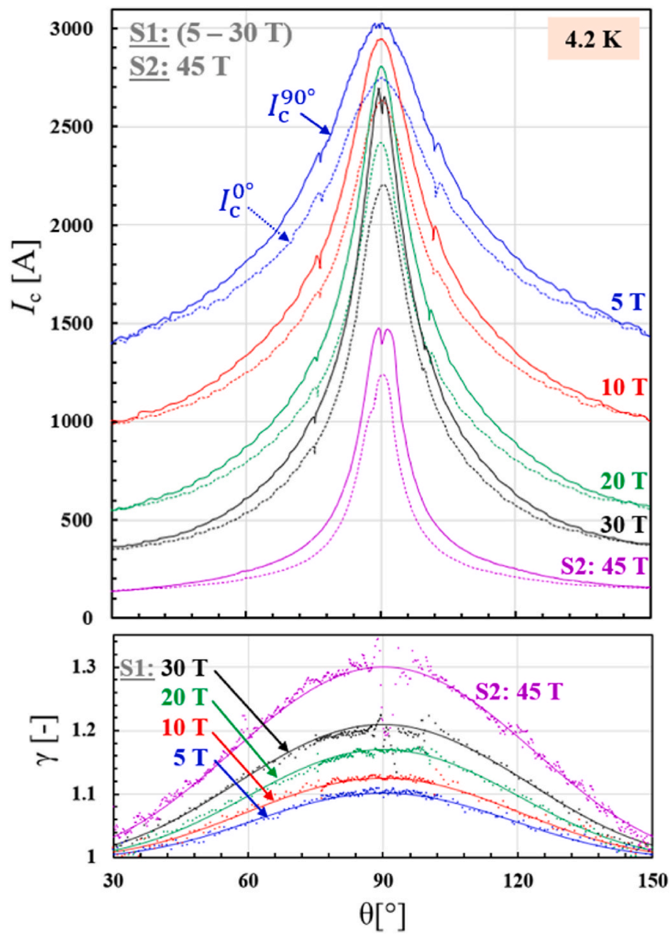

Fig. 10. *Principal critical currents, $I_c^{90^\circ}$ (full lines) and $I_c^{0^\circ}$ (broken lines) of the commercial REBCO tapes S1 and S2 evaluated from torque magnetometry measurements. Sample S1 was measured using probe #1 in applied magnetic fields of 5 - 30 T and S2 using probe #2 at 45 T. All measurements were performed at 4.2 K. The lower part of the image shows the anisotropy ratio $\gamma(\theta)$ evaluated from the torque data using a quadratic function.*

8. Conclusions

We have demonstrated a method that extends standard 2D angular scans $I_c(\theta)$ to 3D anisotropy characterisation $I_c(\theta, \varphi)$ of the REBCO CCs using advanced torque magnetometry probes allowing complete anisotropy mapping (Fig. 12). The presented analytical framework and experimental measurements focused on principal field anisotropies, i.e. at maximum ($\varphi = 0^\circ$) and variable ($\varphi = 90^\circ$) Lorentz force configurations denoted as $I_c^{0^\circ}(\theta)$ and $I_c^{90^\circ}(\theta)$.

The effects of sample geometry, current redistribution, and intrinsic longitudinal–transverse anisotropy were analysed and incorporated to improve the accuracy of the measured critical currents. The experimental measurements were performed at a temperature of 4.2 K and magnetic fields up to 45 T. It was observed that the ratio between the principal critical currents follows higher-order angular dependence and increases with the magnetic field. The presented torque magnetometry based method offers a rapid, non-destructive alternative to transport-based angular characterization of REBCO CCs for high-field environments. Furthermore, the ability of advanced torque magnetometry to characterize 3D anisotropy $I_c(\theta, \varphi, B, T)$ provides essential input for

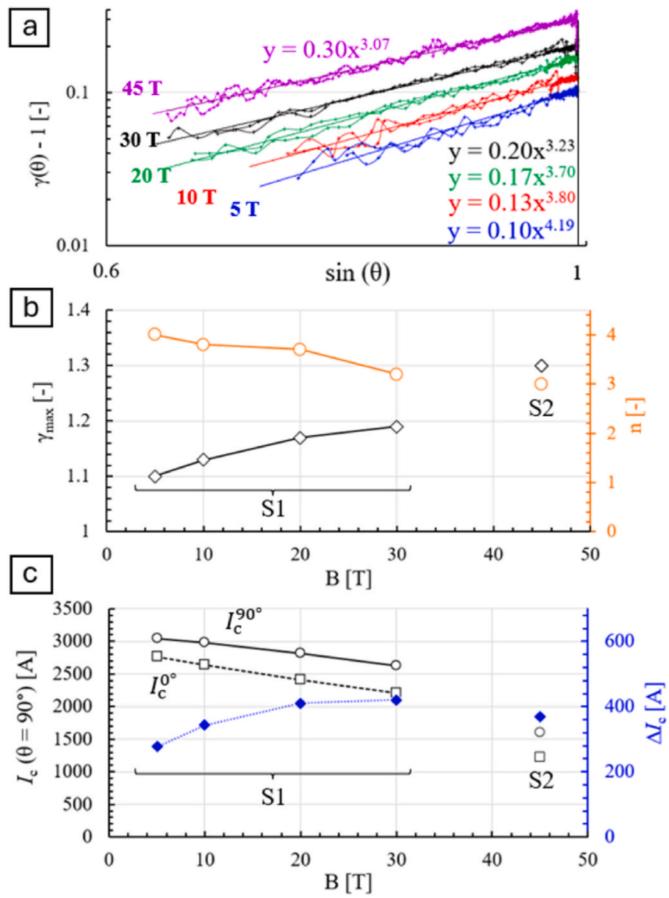

Fig. 11. *The evaluated dependences for sample S1 measured at magnetic fields of 5-30 T and S2 measured at 45 T. a) log–log plot of $\gamma(\theta)-1$ versus $\sin(\theta)$ with the corresponding power function fits. b) field dependence of γ_{max} (primary axis) and the n-exponent (secondary axis) extracted from the power function fits. c) field dependence of peak critical currents $I_c^{0^\circ}$ ($\theta = 90^\circ$) and $I_c^{90^\circ}$ ($\theta = 90^\circ$) (primary axis) and ΔI_c (90°) (secondary axis).*

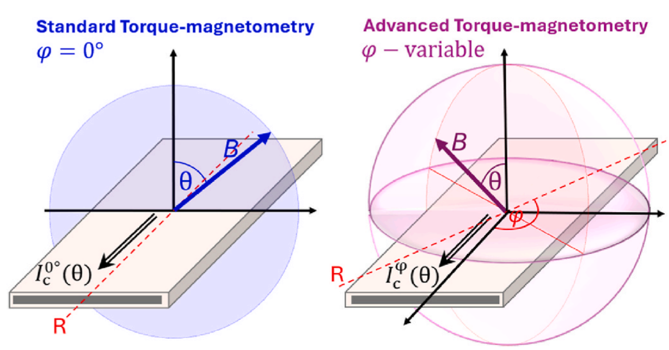

Fig. 12. *The comparison between the standard and advanced torque-magnetometry capability for angular critical current anisotropy characterisation of REBCO CCs. The advanced torque-magnetometry allows full 3D control of magnetic field orientation $I_c(\theta, \varphi)$.*

designing a high field magnet systems and modelling of AC losses for practical superconducting devices.

CRediT authorship contribution statement

R. Ries: Writing – review & editing, Writing – original draft, Visualization, Validation, Software, Methodology, Investigation, Formal analysis, Data curation. **J. Jaroszynski:** Writing – review & editing, Visualization, Validation, Supervision, Software, Resources, Project administration, Methodology, Investigation, Funding acquisition, Formal analysis, Data curation, Conceptualization. **D.C. Larbalestier:** Writing – review & editing, Validation, Supervision, Resources, Project administration, Methodology, Investigation, Funding acquisition, Formal analysis, Data curation, Conceptualization.

Declaration of competing interest

The authors declare that they have no known competing financial interests or personal relationships that could have appeared to influence the work reported in this paper.

Acknowledgements

This work benefitted from many discussions within the broader REBCO effort in the Applied Superconductivity Center and discussions with D. Abraimov, Ch. Tarantiny and J. Bang are particularly noted. Primary support came from a UCGP grant from the National High Magnetic Field Laboratory, which is supported by the National Science Foundation Cooperative Agreement No. DMR-2128556 and by the State of Florida. Secondary support came from the Office of Fusion Energy Sciences Grant DE-SC0022011.

References

[1] Uglietti D. A review of commercial high temperature superconducting materials for large magnets: from wires and tapes to cables and conductors. Supercond Sci Technol 2019;32(5):053001. https://doi.org/10.1088/1361-6668/ab06a2.
[2] Mitchell N, et al. Superconductors for fusion: a roadmap. Supercond Sci Technol 2021;34:103001. https://doi.org/10.1088/1361-6668/ac0992.
[3] Li X, et al. REBCO coated conductors: enabling the next generation of tokamak reactors. Supercond Sci Technol 2025;38:033001. https://doi.org/10.1088/1361-6668/ada9d2.
[4] Molodyk A, et al. Development and large volume production of extremely high current density YBa2Cu3O7 superconducting wires for fusion. Sci Rep 2021;11. https://doi.org/10.1038/s41598-021-81559-z. 2084.
[5] Usoskin A, et al. Long-length YBCO coated conductors for ultra-high field applications: gaining engineering current density via pulsed laser deposition/alternating beam-assisted deposition route. Supercond Sci Technol 2019;32: 094005. https://doi.org/10.1088/1361-6668/ab2cba.
[6] Hartwig Z, et al. VIPER: an industrially scalable high-current high-temperature superconductor cable. Supercond Sci Technol 2020;33(8pp). https://doi.org/10.1088/1361-6668/abb8c0. 11LT01.
[7] Branch P, Osamura K, Hampshire D. Weak emergence in the angular dependence of the critical current density of the high temperature superconductor coated conductor REBCO. Supercond Sci Technol 2020;33:104006. https://doi.org/10.1088/1361-6668/abaebe.
[8] Senatore C, Bonura M, Bagni T. REBCO tapes for applications in ultra-high fields: critical current surface and scaling relations. Supercond Sci Technol 2024;37: 115013. https://doi.org/10.1088/1361-6668/ad7f95.
[9] Senatore C, Barth Ch, Bonura M, Kulich M, Mondonico G. Field and temperature scaling of the critical current density in commercial REBCO coated conductors. Supercond Sci Technol 2016;29:014002. https://doi.org/10.1088/0953-2048/29/1/014002.
[10] Xu A, et al. Angular dependence of Jc for YBCO coated conductors at low temperature and very high magnetic fields. Supercond Sci Technol 2010;23(7pp): 014003. https://doi.org/10.1088/0953-2048/23/1/014003.
[11] Francis A, Abraimov D, Viouchkov Y, Su Y, Kametani F, Larbalestier DC. Development of general expressions for the temperature and magnetic field dependence of the critical current density in coated conductors with variable properties. Supercond Sci Technol 2020;33:044011. https://doi.org/10.1088/1361-6668/ab73ee.
[12] Zhang Z, Zho B, Liu J, Wang L, Wang Q. Engineering-based design and fabrication procedure for mid-temperature REBCO magnets accommodating the strong Ic anisotropy. Superconductivity 2022;1:100005. https://doi.org/10.1016/j.supcon.2022.100005.
[13] Hartwig Z, et al. The SPARC toroidal field model coil program. IEEE Trans Appl Supercond 2024;34:1–16. https://doi.org/10.1109/TASC.2023.3332613.
[14] Whyte DG, et al. Experimental assessment and model validation of the SPARC toroidal field model coil. IEEE Trans Appl Supercond 2024;34:0600218. https://doi.org/10.1109/TASC.2023.3332823.
[15] Wimbush SC, Strickland NM, Long NJ. In-plane field angle dependence of the critical current of RBCO wires at low temperatures. Phys Procedia 2016;81:81–4. https://doi.org/10.1016/j.phpro.2016.04.032.
[16] Weigand M, Rutter NA, Sahonta S-L, Durrell JH. Critical current densities of MOCVD tapes for different current directions. IEEE Trans Appl Supercond 2011;21 (3). https://doi.org/10.1109/TASC.2010.2082477.

[17] Clem JR, Weigand M, Durrell JH, Campbell AM. Theory and experiment testing flux-line cutting physics. Supercond Sci Technol 2011;24(10pp):062002. https://doi.org/10.1088/0953-2048/24/6/062002.
[18] Weigan M, Rutter NA, Durrell JH. In-plane critical current density measurements of straight and curved tracks in RABiTS-MOD coated conductors. Supercond Sci Technol 2013;26(6pp):105012. https://doi.org/10.1088/0953-2048/26/10/105012.
[19] Nie X, Peng J, Xie Y, Yu G, Liu K, Zhu C. FOCUS-HTS: a new stellarator coil design code for three-dimensional high-temperature superconducting magnets. Nucl Fusion 2025;65(14pp):086008. https://doi.org/10.1088/1741-4326/ade697.
[20] Zhou B, Zhang Z, Liu Q, Zhang X, Strickland N, Suo H, Wang L, Liu J, Wang Q. Anisotropic in-plane field angle dependence of critical current in commercial REBCO tapes and its impact on toroidal field magnet for compact tokamak fusion device. Supercond Sci Technol 2025;38:015016. https://doi.org/10.1088/1361-6668/ad9ad6.
[21] Hopkins SC, Woźniak M, Glowacki BA, Chen Y, Kesgin I, Selvamanickam V. Two-axis magnetic field orientation dependence of critical current in full-width REBCO coated conductors. Phys Procedia 2012;36:582–7. https://doi.org/10.1016/j.phpro.2012.06.171.
[22] Strickland NM, Hoffmann C, Wimbush SC. A 1 kA-class cryogen-free critical current characterization system for superconducting coated conductors. Rev Sci Instrum 2014;85:113907. https://doi.org/10.1063/1.4902139.
[23] Jaroszynski J, Constantinescu A-M, Miller G, Larbalestier DC. Magnetometer for large magnetic moments with strong magnetic anisotropy, US patent US12181540B2. 2022.
[24] Jaroszynski J, Constantinescu A-M, Miller G, Xu A, Francis A, Murphy T, Larbalestier DC. Rapid assessment of REBCO CC angular critical current density Jc (B, T = 4.2 K, θ) using torque magnetometry up to at least 30 tesla. Supercond Sci Technol 2022;35:095009. https://doi.org/10.1088/1361-6668/ac8318.
[25] Jaroszynski J, Constantinescu A-M, Bond DK, Francis A, Xu A, Ries R, Bradford G, Bang J, Lee J, Larbalestier D. Critical current, lengthwise fluctuations, and flux jumps in REBCO CC: a torque magnetometry study up to 45 T. arXiv:2502 02706 2025. https://doi.org/10.48550/arXiv.2502.02706.
[26] Brandt EH, Indenbom MV, Forkl K. Type-II superconducting strip in perpendicular magnetic field. EPL 1993;22:735. https://doi.org/10.1209/0295-5075/22/9/017.
[27] Lao M, Bernardi J, Bauer M, Eisterer M. Critical current anisotropy of GdBCO tapes grown on ISD–MgO buffered substrate. Supercond Sci Technol 2015;28:124002. https://doi.org/10.1088/0953-2048/28/12/124002.
[28] Pompeo N, et al. Intrinsic anisotropy and pinning anisotropy in nanostructured YBa2Cu3O7−δ from microwave measurements. Supercond Sci Technol 2020;33:044017. https://doi.org/10.1088/1361-6668/ab773b.
[29] Zhang Y, et al. Magnetic field orientation dependence of flux pinning in (Gd,Y) Ba2Cu3O7−x coated conductor with tilted lattice and nanostructures. Phys C Supercond 2009;469:23–4. https://doi.org/10.1016/j.physc.2009.08.007.
[30] Strickland NM, et al. Onset temperature of intrinsic pinning in a REBCO coated conductor from critical current anisotropy. Superconductivity 2022;4:100025. https://doi.org/10.1016/j.supcon.2022.100025.